ACS Photonics

Article

pubs.acs.org/journal/apchd5

Crystalline Silicon Optical Fibers with Low Optical Loss

Subhasis Chaudhuri,[†,∥,#] Justin R. Sparks,[†,∥,□,#] Xiaoyu Ji,[§,∥] Mahesh Krishnamurthi,[§,∥] Li Shen,[⊥] Noel Healy,[⊥,△] Anna C. Peacock,[⊥] Venkatraman Gopalan,[§,∥] and John V. Badding*[,†,‡,§,∥]

[†]Department of Chemistry, [‡]Department of Physics, [§]Department of Materials Science and Engineering, and [∥]Materials Research Institute, Pennsylvania State University, University Park, Pennsylvania 16802, United States

[⊥]Optoelectronics Research Centre, University of Southampton, Southampton, SO17 1BJ, U.K.

[△]Emerging Technology and Materials Group, School of Electrical and Electronic Engineering, Newcastle University, Newcastle upon Tyne NE1 7RU, U.K.

[□]Department of Chemistry, Muhlenberg College, Allentown, Pennsylvania 18104, United States

ABSTRACT: Polycrystalline silicon core optical fibers have been fabricated by modified thermal annealing of amorphous silicon chemically deposited at high pressure. The resulting fibers have small-diameter cores, a geometry advantageous for optical guidance. Moreover, the combination of chemical deposition and annealing avoids difficulties associated with undesired transfer of oxygen impurities to the silicon core from the molten cladding during the drawing process. The high aspect ratio of the amorphous silicon core and the presence of the silica cladding surrounding make the design rules for annealing to optimize their polycrystalline structure different from those of conventional amorphous silicon films. We find that optimization of the annealing allows for an increase in the polycrystalline grain size and decrease in the defects in the silicon core. A low optical loss of less than 1 dB/cm at a wavelength of 2.2 μm is thus realized, much lower than that reported for small core size (<10 μm) crystalline silicon fibers and comparable to the loss in many planar semiconductor waveguides. This loss is just below the threshold of 1 dB/cm often considered necessary for many photonic and optoelectronic applications at near to mid-infrared wavelengths in areas such as nonlinear photonics, lasers, and in-fiber photodetectors. Further reduction in optical losses as deposition and annealing techniques are improved can be anticipated.

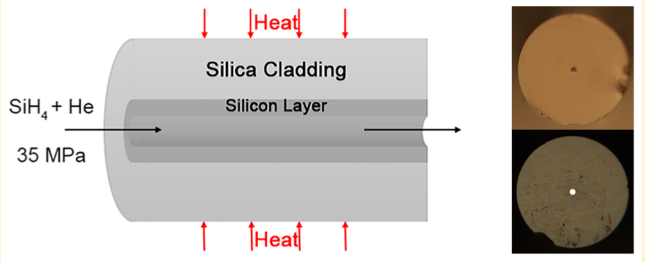

KEYWORDS: *optical fiber, silicon photonics, thermal annealing, crystal growth, confined geometry deposition, chemical vapor deposition, high pressure*

Conventional silica optical fibers have had a large range of scientific and technological impacts.[1] A new class of fibers with crystalline semiconductor cores is now emerging.[2−5] Fabrication of these fibers is motivated by the advantageous photonic and electronic properties of crystalline semiconductors for many applications. Depending on the semiconductor, these advantages include transparency over a wide range of wavelengths into the mid- and far-infrared, large nonlinear optical coefficients, and high damage thresholds.[4] Silica fibers have high optical losses at mid-infrared wavelengths longer than 2.5 μm, while soft glass infrared chalcogenide fibers generally can guide only modest optical powers.[6,7] Crystalline semiconductor optical fibers may allow for the guidance of high optical powers with low optical losses at wavelengths well into the far-infrared, a capability desirable for many industrial, scientific, and medical applications.[7] In-fiber semiconductor electronic junctions for applications such as high-speed in-fiber detectors and flexible and permeable woven solar fabrics have been demonstrated.[4,8] Light-emitting devices based on these junctions that share the advantageous thermal and gain properties of fiber lasers may ultimately be possible.[8−12] The challenge of realizing low optical loss for small-diameter cores fabricated from the technologically important unary semiconductors has largely not yet been met. Small core diameters on the order of a few micrometers or less have the important property of allowing for low-order or single-mode guidance of light, depending on the refractive index of the chosen cladding.

Several different approaches toward the fabrication of silicon fibers have been reported. The first was high-pressure chemical vapor deposition (HPCVD), which employs high pressures of silane (MPa to tens of MPa) to deposit layers and wires of silicon into small silica capillaries and microstructured optical fiber (MOF) templates.[13−15] The silicon fiber cores fabricated in this way can be near atomically smooth[16] and void-free and have diameters in the range of hundreds of nanometers to tens of micrometers.[17] HPCVD can deposit hydrogen-free amorphous silicon that can be annealed to form a crystalline core.[16,18] Powder-in-tube[19] and molten core drawing approaches[20] to the fabrication of crystalline silicon core fibers have also been reported. These techniques require the silicon core to be molten while the silica cladding softens during

Received: August 4, 2015
Published: January 12, 2016

DOI: 10.1021/acsphotonics.5b00434
ACS Photonics 2016, 3, 378−384

fabrication. Oxygen can thus be incorporated into the silicon core from the silica cladding, which has driven the development of gettering techniques.[21] An alkaline earth oxide interface layer between the silicon core and silica cladding has also been used for scavenging the oxygen from the core.[22] Using this technique 10 μm diameter silicon core fibers have been fabricated, but low optical loss has been reported only in cores larger than 65 μm. Small lengths of silicon nanofibers have been made by repeated drawing of large-core fibers,[23] and fibers with micrometer-sized silicon cores have also been fabricated by using aluminum to reduce silica into silicon during the drawing process,[24] but optical transmission has not been demonstrated in either of these fibers. Furthermore, a pressure-assisted melt filling technique has been used to infiltrate hollow pores inside fibers with different materials such as germanium[25] and arsenic sulfide[26,27] for applications in near-field scanning optical microscope tips, supercontinuum generation, etc. However, this approach is challenging to apply to silicon owing to its relatively high melting temperature.

Here we report that a properly designed annealing strategy can reduce the optical loss at mid-infrared wavelengths of small-core silicon optical fibers deposited by HPCVD to below 1 dB/cm, which is often considered a threshold for practical application of semiconductor planar waveguides. Although annealing techniques have been widely studied in silicon films, much less effort has been focused on their application to the cylindrical optical fiber geometry. The unique one-dimensional geometry of optical fibers and the presence of a silica cladding that completely surrounds the silicon core (in contrast to the typical presence of silica on only one side of a film) make annealing of silicon fibers potentially different from that of silicon films. The dominant loss mechanism in annealed polycrystalline fibers is scattering from grain boundaries. Thus, increases in grain size arising from optimized annealing approaches have considerable potential to decrease optical loss. Further development of the techniques reported here may allow for large single crystals, millimeters in length or more, in silicon fiber cores deposited by HPCVD that allow for even lower optical losses.

Chemical vapor deposition in the two-dimensional planar geometry is much more common than in the one-dimensional fiber geometry. Deposition of amorphous planar silicon films followed by crystallization has been reported to be a better strategy to realize low optical losses and good material quality than direct deposition of polycrystalline films.[28] For this reason polycrystalline silicon made by this technique is generally deposited in amorphous form and then annealed.[29] Several different techniques can be used to deposit amorphous silicon films including low-pressure chemical vapor deposition (LPCVD),[30] atmospheric pressure chemical vapor deposition (APCVD),[31] plasma-enhanced chemical vapor deposition (PECVD),[32] and others. LPCVD silicon, used in many technological applications, is typically deposited amorphous at 540−550 °C, as it deposits crystalline films at temperatures higher than 580 °C.[33] The temperature at which crystalline domains nucleate in these LPCVD amorphous films varies depending on experimental parameters such as thickness and deposition conditions, but is usually between 550 and 600 °C.[34] At 550 °C incipient small crystallites form in LPCVD films, whose number increases with further increase in temperature.[34−36] As annealing progresses, these crystallites serve as nuclei for crystal growth that gradually consumes the amorphous material surrounding them. This process continues until the growing crystals merge.[33] Lower annealing temperatures increase the mean grain size at the expense of slower grain growth.[34]

Many planar silicon films are deposited on silica, and thus the impact of the interface between the substrate and the film must also be considered. The interface is a preferred site for nucleation.[29,37] Stress can accumulate at this interface because of the volume contraction associated with the crystallization of silicon and hindered mobility of silicon atoms bound to SiO_2 at the interface. Stress-induced defects are formed such as microtwins and dislocations. These defects can be eliminated by heating above 750 °C.[38] Recrystallization of grains, which is advantageous to further increase their size, does not happen appreciably at temperatures below 1000 °C and accelerates as the temperature increases above 1200 °C.[39,40] Fortunately, in contrast to most planar electronic devices, HPCVD-grown amorphous silicon optical fibers can withstand temperature as high as 1300 °C for ∼10 min without deformation of the silica cladding. Thus, it seems a two-step annealing process should be best for the formation of large grains in these fibers. Appropriate low-temperature annealing should ideally lead to the nucleation of a few grains that grow in size and merge as the temperature is increased. A subsequent high-temperature annealing should allow for further increase in size via recrystallization.

Several silicon fiber cores were deposited via HPCVD inside 5.6 μm diameter silica capillaries (Figure 1). To determine the temperature at which silicon crystallizes, it was deposited at temperatures ranging from 361 to 665 °C. Raman spectra collected with 633 nm excitation reveal that the silicon fiber core is amorphous until the deposition temperature is raised to 519 °C (Figure 2). Thus, for crystallization experiments the deposition temperature was kept in the range of 480−500 °C, low enough to deposit amorphous silicon but high enough to avoid incorporation of hydrogen. Hydrogenated amorphous silicon shrinks more than amorphous silicon during annealing and thus can separate from the silica cladding. This crystallization temperature of 519 °C is considerably lower than that (>550 °C) of amorphous LPCVD silicon films. Ascertaining the details of the origin of this lower crystallization temperature will likely require further investigation. Stress,[33] surface physics and chemistry,[33] and the cylindrical fiber geometry may all play a role. Raman spectroscopic investigations reveal that stresses of a few tenths of a GPa to a GPa or more consistently arise as a result of the volume contraction of amorphous silicon upon crystallization inside a fiber template and also as a result of thermal expansion mismatch between the silica cladding and the silicon core.[13,41,42] The high-purity silica

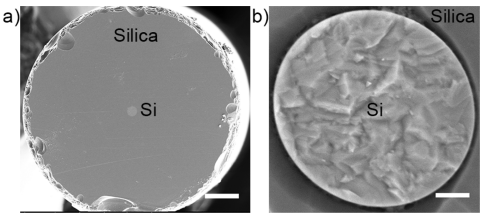

Figure 1. (a) Field emission scanning electron microscope (FESEM) image of a 5.6 μm silicon core optical fiber. (b) FESEM image of the polycrystalline silicon core. The silica cladding has been partially etched out from the sides with hydrofluoric acid to reveal the silicon core Scale bars: (a) 20 μm; (b) 1 μm.

DOI: 10.1021/acsphotonics.5b00434
ACS Photonics 2016, 3, 378−384

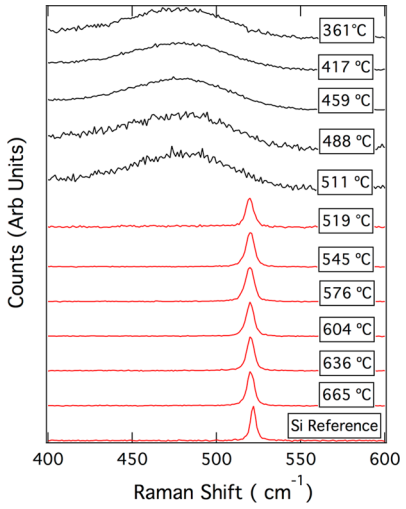

Figure 2. Raman spectra of silicon fiber cores after deposition at different temperatures. Crystallization begins at 519 °C. The positions of the crystalline silicon Raman modes are downshifted from a silicon reference by 1.5 to 2 cm^{-1}. This downshift can be attributed to tensile stress arising from the difference in the thermal expansion coefficients between silica and silicon (see ref 13).

of the fiber template may have fewer hydroxyl groups than most silica planar substrates, which can impact surface chemistry. Furthermore, the silica fiber template surrounds the silicon core such that nuclei that facilitate crystallization should completely surround it.[33]

To investigate the hypothesis that a two-step annealing process will give the largest and most defect-free grain growth, two identical amorphous silicon fibers were annealed for 3 days at temperatures of 530 and 560 °C, respectively (slightly and somewhat above the onset temperature for crystallization). These two fibers were then annealed at 1300 °C for 10 min to remove defects and allow for recrystallization. A third control sample was annealed only at 1300 °C for 10 min. Raman spectra of these three samples collected using an excitation wavelength of 633 nm are shown in Figure 3. The first-order A_{1g} Raman peaks at 520 cm^{-1}, characteristic of crystalline silicon, were fit with a Voigt profile to separate the Lorentzian Raman component from the Gaussian instrument component. A silicon single-crystal reference was found to have a Lorentzian fwhm of 2.6 cm^{-1} at ambient temperature, in good agreement

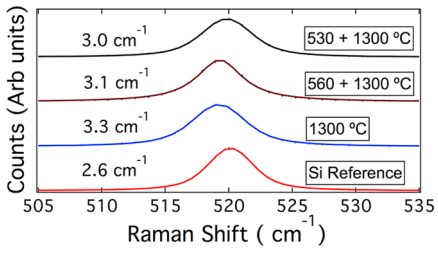

Figure 3. Raman spectra of polycrystalline silicon cores after annealing at different temperatures and a single-crystal silicon reference wafer. The fwhm's of the Lorentzian Raman component of the peaks are shown. The experimental data are plotted as dots, and the fits are shown as solid lines. Downshifts in the Raman peak position from a reference wafer were small, ranging from 0.3 to 0.9 cm^{-1}, again associated with tensile stress but smaller in magnitude than is found for crystalline silicon fibers deposited directly at lower temperatures.

with previous reports.[43] The control sample annealed at only 1300 °C has a fwhm of 3.3 cm^{-1}, the sample annealed at 560 and 1300 °C has a smaller fwhm of 3.1 cm^{-1}, and the one annealed at 530 and 1300 °C has the smallest fwhm, 3.0 cm^{-1}. This peak width for the latter sample is closest to that of the single-crystal reference, indicating that it likely has the largest and most defect-free crystalline domains.

To gain further insight into the grain structure and crystal growth of the silicon core during annealing, TEM (transmission electron microscopy) images were collected on a sample annealed first at 530 °C. Small crystals and a few large crystals are observed (Figure 4a), along with many dislocation defects

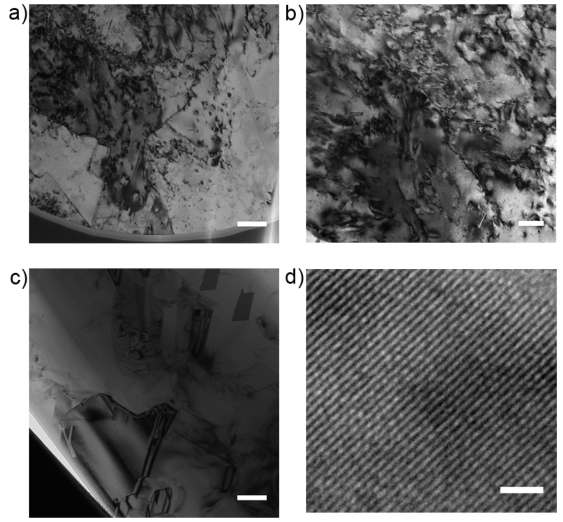

Figure 4. (a) TEM image of a section of polycrystalline Si core annealed to crystallize it at 530 °C, revealing relatively small grains. (b) Many defects such as dislocations are in a single grain of this same fiber core. (c) TEM image of the same Si fiber core after high -temperature annealing at 1300 °C, revealing growth of much larger grains and a reduction in defect density. (d) HRTEM image of a grain in the sample after high-temperature anneal revealing a (111) lattice plane. Scale bars: (a) 250 nm; (b) 100 nm; (c) 250 nm; (d) 2 nm.

(Figure 4b) that are thought to arise to relieve stress that appears at the Si−SiO_2 interface. TEM images of this sample collected after the second high-temperature annealing at 1300 °C exhibit many fewer dislocation defects (Figure 4c). The silicon fiber core is now composed of large grains of silicon; some of these grains are micrometers in size, consistent with the small fwhm observed in the Raman spectra collected on this sample. High-resolution TEM images of this high-temperature-annealed sample reveal crystalline lattice planes (Figure 4d). Thus, TEM analysis supports the hypothesis that a 530 °C low-temperature anneal followed by a 1300 °C high-temperature anneal is advantageous in producing large-size grains with few defects.

Silicon has a band gap of 1.1 eV and low optical loss at wavelengths from 1.2 to 6 μm. At 1.55 μm wavelength the refractive indices of crystalline silicon and silica are 3.48 and 1.44, respectively. For a 5.6 μm diameter fiber core the numerical aperture (NA) is high, 3.17, and the V number is 36 such that the fiber can support a few hundred modes. However, it is straightforward to optimize coupling to preferentially launch into the fundamental mode.[44] Optical transmission losses are of paramount importance to the performance of silicon core optical fibers and are also a good measure of the

DOI: 10.1021/acsphotonics.5b00434
ACS Photonics 2016, 3, 378−384

silicon material quality. Losses were measured at 1.55 μm by a standard cutback technique. Fibers annealed solely at 530 °C exhibit losses of 27 dB/cm, which decrease to 13 dB/cm for those annealed solely at 560 °C. High loss values are expected for these fibers because they have small grain sizes, many defects, and amorphous regions. However, after the second anneal of the 530 °C fiber at 1300 °C, the optical loss decreases to 5.2 dB/cm, the lowest value yet reported for a small-core crystalline silicon fiber. This lower loss is consistent with the large grain size and small defect density observed in TEM images. The second anneal at 1300 °C for the 560 °C fiber improves the loss to only 11 dB/cm. Finally, the loss for a fiber annealed solely at 1300 °C with no prior low-temperature anneal is 10 dB/cm. This value offers a slight improvement over the loss measured for the fiber annealed at 560 °C and that measured when this fiber is annealed a second time at 1300 °C. We conclude that the two-step annealing process is most useful when the low-temperature anneal is performed close to the lowest crystallization temperature of 519 °C. This observation supports the hypothesis that appropriate low-temperature annealing should lead to the nucleation of a few grains that grow in size and merge as the temperature is increased to give the lowest optical loss. The optical losses observed at 1.55 μm upon using different annealing strategies are summarized in Table 1.

Table 1. Optical Loss Values of Silicon Fibers Annealed at Different Temperatures

annealing temperature (°C)	optical loss at 1.55 μm (dB/cm)
530	27
560	13
1300	10
560 followed by 1300	11
530 followed by 1300	5.2

The optical loss at different wavelengths was measured on the sample annealed at 530 and then 1300 °C, which gave the lowest optical loss at 1.55 μm. It could be fit by a function that varied as $\lambda^{-3.6}$ (Figure 5). A λ^{-4} functional dependence is

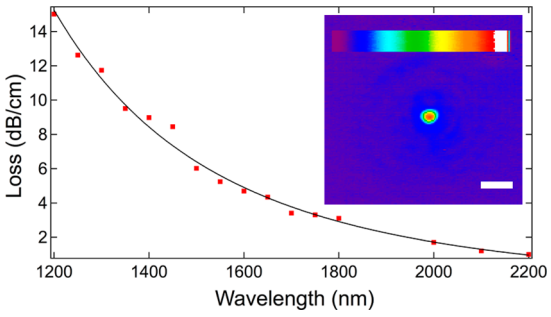

Figure 5. Optical loss vs wavelength for the sample annealed at 530 °C and then 1300 °C fit to $\lambda^{-3.6}$. Inset shows the output mode at 1.55 μm. Scale bar: 10 μm.

characteristic of Rayleigh scattering. Thus, the major source of optical loss in this fiber appears to arise from scattering at the grain boundaries. Although some of the grains are micrometers in size, it can be expected that defects near the grain boundaries are much smaller than the wavelengths used in this study, giving rise to Rayleigh scattering as observed.[45] The lowest measured optical loss is 0.99 dB/cm at 2.2 μm wavelength, the lowest value reported for a small-core polycrystalline silicon fiber. Thus, this fiber has potential application as a waveguide in near- and mid-infrared regions.

The annealed silicon fibers can also be used in the fabrication of in-fiber devices for optoelectronic applications. For example, a 1 cm long polycrystalline silicon fiber that has been annealed at 530 and 1300 °C can be used as a field effect transistor (FET). The silica at the two ends of the fiber was etched away to reveal the silicon for source and drain contacts, respectively. The coaxial silica cladding was configured as a gate. With zero gate voltage, V_g = 0, the measurement corresponds to a two-terminal I_{drain}–V_{source} sweep, showing the silicon core is continuous and electrically active, with an electrical conductivity of 1.41 × 10^{-2} S cm^{-1}. As V_g is varied from −100 to +100 V, the gradient of the I_{drain}–V_{source} curve increases, as shown in Figure 6, indicating that the carriers in the silicon core

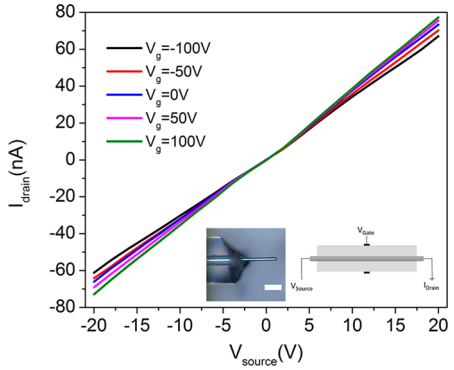

Figure 6. Three-terminal electrical measurement on the annealed Si fiber. The current voltage characteristics of the FET show the effect of bias applied at the gate. The left inset shows an optical image of an etched end of the silicon fiber. Scale bar: 50 μm. Right inset shows schematic of the FET.

are *n* type. The effect of V_g on the conductance gives an estimation of the free-carrier concentration of 1.7 × 10^{16} cm^{-3}. The silicon fiber is also photoconductive, as the conductivity increases when illuminated with 488 nm light (Figure 7).

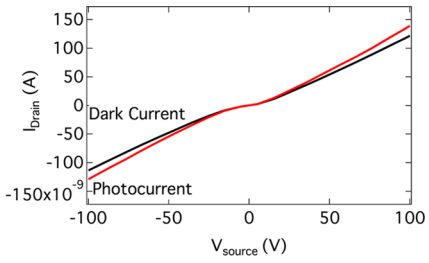

Figure 7. Photoconductance characteristic of the silicon fiber. The current increases when illuminated with 488 nm light.

The low optical loss observed for these electrically active polycrystalline silicon fibers annealed in a two-step process should improve their performance in nonlinear applications, allowing for the development of compact all-optical modulators, switches, and Raman amplifiers that can operate well into the mid-infrared wavelength regime. Several of these applications have already been demonstrated in silicon waveguides with micrometer-sized dimensions, both in planar[46] and fiber geometries.[47] Infrared fiberscopes capable of imaging in the infrared with high spatial resolution will also benefit from

DOI: 10.1021/acsphotonics.5b00434
ACS Photonics 2016, 3, 378−384

these reduced optical losses. There is also much interest in improving the performance of polycrystalline junction-based in-fiber detectors and solar fabrics, which should be facilitated by the improved silicon materials quality enabled by two-step annealing.

METHODS

High-Pressure Chemical Vapor Deposition. Silane (SiH_4) was used as a precursor and helium as a carrier. This mixture under a total pressure of 35 MPa is introduced into a hollow core silica fiber (core size of 5.6 μm diameter) that is kept at a temperature of 480−500 °C. Under these conditions silane undergoes several coupled reactions to finally decompose into amorphous silicon. The silicon is deposited as a smooth conformal film in the silica capillary to form a fully filled step index fiber.

Characterization. Field emission electron microscope images were collected using a FEI Nova NanoSEM 630 FESEM. Raman spectra of the fibers were collected with a Renishaw Invia Raman microscope. For TEM characterization the silica cladding of the fiber was etched away with hydrofluoric acid, and the remaining silicon core was thinned with a FEI Quanta 200 3D Dual Beam focused ion beam system. The fiber was then imaged using a Philips (FEI) EM420T transmission electron microscope. High-resolution TEM images were collected with a JEOL EM-2010 microscope. To measure optical loss, the samples were mounted in larger capillaries and polished on both ends. The optical transmission was then measured using the cut-back technique over a range of wavelengths from the near-infrared to mid-infrared regime. Three laser sources including a supercontinuum (Fianium SC-400), a pigtailed laser diode, and a continuous wave tunable Cr^{2+}:ZnSe laser were used to access wavelengths of 1.3−1.8, 1.55, and 2−2.2 μm. The output power of the supercontinuum source was kept very low to minimize the nonlinear effects in the polycrystalline Si core fiber. The light was launched into the fiber core via free space coupling using a 40× magnification microscope objective lens, and a second 40× objective was used to capture the transmitted light and focus it onto a germanium photodiode or lead selenide (PbSe) detector depending on the wavelength.

For electrical and photoconductivity experiments a 1 cm long polycrystalline silicon fiber annealed at 530 and 1300 °C was used. The ends of the fiber were etched away with hydrofluoric acid to expose the bare silicon core. These ends were then coated with aluminum to make contacts. In−Ga eutectic droplets were used to increase the contact area of the two fiber ends, which were connected to a Keithley 6430 source meter through a probe station. These ends acted as the source and drain, respectively. For photoconductivity measurement an argon ion laser emitting at 488 nm was used to illuminate the fiber while performing a two-terminal $I_{drain}-V_{source}$ sweep. In the FET measurement, another In−Ga droplet about 1 mm in size was used as the gate contact and connected to another source meter to apply gate voltages.

Calculations.

Numerical aperture (NA) of the fiber at 1.55 μm

$$= (n_{core}{}^2 - n_{cladding}{}^2)^{1/2} = 3.17$$

where the refractive index of silica ($n_{cladding}$) = 1.44 and the refractive index of silicon (n_{core}) = 3.48.

$$\text{V number} = 2\pi(a/\lambda) \times \text{NA} = 36$$

where a is the radius of the core (2.8 μm) and λ is the wavelength (1.55 μm).

Number of modes supported by the fiber at 1.55 μm $\approx V^2/2$ = 648

Conductivity:

$$\sigma = 1/\rho = L/(R\pi r^2) = 1/(2.872 \times 10^8 \Omega \times \pi(2.8 \times 10^{-4}\ \text{cm})^2) = 1.41 \times 10^{-2}\ \text{S·cm}^{-1}$$

where resistance of the fiber $R = 2.872 \times 10^8\ \Omega$, fiber length L = 1 cm, and cross-sectional area = $\pi r^2 = \pi(2.8 \times 10^{-4}\text{cm})^2$

Carrier concentration:

$$N_e = CV_{pinch\text{-}off}/\pi e r^2 L$$

where capacitance per unit length $C/L \approx 2\pi\varepsilon\varepsilon_0/\ln(2h/r)$, ε is relative permittivity of fused silica, and h is the thickness of the silica cladding.

$$C/L = 2\pi \times 3.75 \times 8.854 \times 10^{-12}/\ln(2 \times 40/2.8) = 6.22 \times 10^{-11}\ \text{F·m}^{-1}$$

$$N_e = 6.22 \times 10^{-11} \times 10^{-6} \times (-1100)/(\pi \times (-1.602 \times 10^{-19}) \times (2.8 \times 10^{-6})^2) = 1.7 \times 10^{16}\ \text{cm}^{-3}$$

AUTHOR INFORMATION

Corresponding Author

*E-mail: jbadding@chem.psu.edu.

Author Contributions

#S. Chaudhuri and J. R. Sparks contributed equally to this work.

Notes

The authors declare no competing financial interest.

ACKNOWLEDGMENTS

We acknowledge Joshua Maier and Dr. Trevor Clark for assistance with sample preparation by means of a focused ion beam and transmission electron microscopy characterization, Dr. Ke Wang for assistance with high-resolution transmission electron microscopy, and Dr. Pier Sazio for help with FET measurements. We acknowledge funding from DARPA PULSE (1550650, MOD5), EPSRC (EP/G051755/1 and EP/J004863/1), the National Science Foundation (DMR-1107894), and the Penn State Materials Research Science and Engineering Center funded by NSF awards DMRs - 0820404 and 1420620 as primary support.

REFERENCES

(1) Gambling, W. A. The rise and rise of optical fibers. *IEEE J. Sel. Top. Quantum Electron.* **2000**, *6*, 1084−1093.

(2) Abouraddy, A. F.; Bayindir, M.; Benoit, G.; Hart, S. D.; Kuriki, K.; Orf, N.; Shapira, O.; Sorin, F.; Temelkuran, B.; Fink, Y. Towards multimaterial multifunctional fibres that see, hear, sense and communicate. *Nat. Mater.* **2007**, *6*, 336−347.

(3) Ballato, J.; Hawkins, T.; Foy, P.; Yazgan-Kokuoz, B.; McMillen, C.; Burka, L.; Morris, S.; Stolen, R.; Rice, R. Advancements in semiconductor core optical fiber. *Opt. Fiber Technol.* **2010**, *16*, 399−408.

DOI: 10.1021/acsphotonics.5b00434
ACS Photonics 2016, 3, 378−384

(4) Sparks, J. R.; Sazio, P. J. A.; Gopalan, V.; Badding, J. V. Templated Chemically Deposited Semiconductor Optical Fiber Materials. *Annu. Rev. Mater. Res.* **2013**, *43*, 527−557.
(5) Peacock, A. C.; Sparks, J. R.; Healy, N. Semiconductor optical fibres: progress and opportunities. *Laser Photonics Rev.* **2014**, *8*, 53−72.
(6) Eggleton, B. J.; Luther-Davies, B.; Richardson, K. Chalcogenide photonics. *Nat. Photonics* **2011**, *5*, 141−148.
(7) Méndez, A.; Morse, T. F. *Specialty Optical Fibers Handbook*; Academic Press: Amsterdam, 2007.
(8) He, R. R.; Sazio, P. J. A.; Peacock, A. C.; Healy, N.; Sparks, J. R.; Krishnamurthi, M.; Gopalan, V.; Badding, J. V. Integration of gigahertz-bandwidth semiconductor devices inside microstructured optical fibres. *Nat. Photonics* **2012**, *6*, 174−179.
(9) Saleh, B. E. A.; Teich, M. C. *Fundamentals of Photonics*, 2nd ed.; Wiley-Interscience: Hoboken, NJ, 2007.
(10) Tao, G.; Stolyarov, A. M.; Abouraddy, A. F. Multimaterial Fibers. *Int. J. Appl. Glass Sci.* **2012**, *3*, 349−368.
(11) Graham-Rowe, D. Fibres get functional. *Nat. Photonics* **2011**, *5*, 66−67.
(12) Sparks, J. R.; He, R.; Healy, N.; Krishnamurthi, M.; Peacock, A. C.; Sazio, P. J. A.; Gopalan, V.; Badding, J. V. Zinc Selenide Optical Fibers. *Adv. Mater.* **2011**, *23*, 1647−1651.
(13) Sazio, P. J. A.; Amezcua-Correa, A.; Finlayson, C. E.; Hayes, J. R.; Scheidemantel, T. J.; Baril, N. F.; Jackson, B. R.; Won, D. J.; Zhang, F.; Margine, E. R.; Gopalan, V.; Crespi, V. H.; Badding, J. V. Microstructured optical fibers as high-pressure microfluidic reactors. *Science* **2006**, *311*, 1583−1586.
(14) He, R.; Day, T. D.; Krishnamurthi, M.; Sparks, J. R.; Sazio, P. J. A.; Gopalan, V.; Badding, J. V. Silicon p-i-n Junction Fibers. *Adv. Mater.* **2013**, *25*, 1461−1467.
(15) Baril, N. F.; He, R. R.; Day, T. D.; Sparks, J. R.; Keshavarzi, B.; Krishnamurthi, M.; Borhan, A.; Gopalan, V.; Peacock, A. C.; Healy, N.; Sazio, P. J. A.; Badding, J. V. Confined High-Pressure Chemical Deposition of Hydrogenated Amorphous Silicon. *J. Am. Chem. Soc.* **2012**, *134*, 19−22.
(16) Healy, N.; Lagonigro, L.; Sparks, J. R.; Boden, S.; Sazio, P. J. A.; Badding, J. V.; Peacock, A. C. Polycrystalline silicon optical fibers with atomically smooth surfaces. *Opt. Lett.* **2011**, *36*, 2480−2482.
(17) Baril, N. F.; Keshavarzi, B.; Sparks, J. R.; Krishnamurthi, M.; Temnykh, I.; Sazio, P. J. A.; Peacock, A. C.; Borhan, A.; Gopalan, V.; Badding, J. V. High-Pressure Chemical Deposition for Void-Free Filling of Extreme Aspect Ratio Templates. *Adv. Mater.* **2010**, *22*, 4605−4611.
(18) Lagonigro, L.; Healy, N.; Sparks, J. R.; Baril, N. F.; Sazio, P. J. A.; Badding, J. V.; Peacock, A. C. Low loss silicon fibers for photonics applications. *Appl. Phys. Lett.* **2010**, *96*.
(19) Scott, B.; Wang, K.; Caluori, V.; Pickrell, G. Fabrication of silicon optical fiber. *Opt. Eng.* **2009**, *48*, 100501.
(20) Ballato, J.; Hawkins, T.; Foy, P.; Stolen, R.; Kokuoz, B.; Ellison, M.; McMillen, C.; Reppert, J.; Rao, A. M.; Daw, M.; Sharma, S.; Shori, R.; Stafsudd, O.; Rice, R. R.; Powers, D. R. Silicon optical fiber. *Opt. Express* **2008**, *16*, 18675−18683.
(21) Morris, S.; Hawkins, T.; Foy, P.; McMillen, C.; Fan, J.; Zhu, L.; Stolen, R.; Rice, R.; Ballato, J. Reactive molten core fabrication of silicon optical fiber. *Opt. Mater. Express* **2011**, *1*, 1141−1149.
(22) Nordstrand, E. F.; Dibbs, A. N.; Eraker, A. J.; Gibson, U. J. Alkaline oxide interface modifiers for silicon fiber production. *Opt. Mater. Express* **2013**, *3*, 651−657.
(23) Gumennik, A.; Wei, L.; Lestoquoy, G.; Stolyarov, A. M.; Jia, X.; Rekemeyer, P. H.; Smith, M. J.; Liang, X.; Grena, B. J.; Johnson, S. G.; Gradecak, S.; Abouraddy, A. F.; Joannopoulos, J. D.; Fink, Y. Silicon-in-silica spheres via axial thermal gradient in-fibre capillary instabilities. *Nat. Commun.* **2013**, *4*, 2216.
(24) Hou, C.; Jia, X. T.; Wei, L.; Tan, S. C.; Zhao, X.; Joannopoulos, J. D.; Fink, Y. Crystalline silicon core fibres from aluminium core preforms. *Nat. Commun.* **2015**, *6*, 6248.
(25) Tyagi, H. K.; Schmidt, M. A.; Prill Sempere, L.; Russell, P. S. Optical properties of photonic crystal fiber with integral micron-sized Ge wire. *Opt. Express* **2008**, *16*, 17227−36.
(26) Granzow, N.; Schmidt, M. A.; Chang, W.; Wang, L.; Coulombier, Q.; Troles, J.; Toupin, P.; Hartl, I.; Lee, K. F.; Fermann, M. E.; Wondraczek, L.; Russell, P. S. Mid-infrared supercontinuum generation in As_2S_3-silica "nano-spike" step-index waveguide. *Opt. Express* **2013**, *21*, 10969−77.
(27) Lee, K. F.; Granzow, N.; Schmidt, M. A.; Chang, W.; Wang, L.; Coulombier, Q.; Troles, J.; Leindecker, N.; Vodopyanov, K. L.; Schunemann, P. G.; Fermann, M. E.; Russell, P. S.; Hartl, I. Midinfrared frequency combs from coherent supercontinuum in chalcogenide and optical parametric oscillation. *Opt. Lett.* **2014**, *39*, 2056−9.
(28) Harbeke, G.; Krausbauer, L.; Steigmeier, E. F.; Widmer, A. E.; Kappert, H. F.; Neugebauer, G. Growth and Physical-Properties of Lpcvd Polycrystalline Silicon Films. *J. Electrochem. Soc.* **1984**, *131*, 675−682.
(29) Bo, X. Z.; Yao, N.; Shieh, S. R.; Duffy, T. S.; Sturm, J. C. Large-grain polycrystalline silicon films with low intragranular defect density by low-temperature solid-phase crystallization without underlying oxide. *J. Appl. Phys.* **2002**, *9*, 2910−2915.
(30) Kamins, T. I.; Mandurah, M. M.; Saraswat, K. C. Structure and Stability of Low-Pressure Chemically Vapor-Deposited Silicon Films. *J. Electrochem. Soc.* **1978**, *125*, 927−932.
(31) Nagasima, N.; Kubota, N. Structures of Si Films Chemically Vapor-Deposited on Amorphous Sio2 Substrates. *Jpn. J. Appl. Phys.* **1975**, *14*, 1105−1112.
(32) Kamins, T. I.; Chiang, K. L. Properties of Plasma-Enhanced Cvd Silicon Films 0.1. Undoped Films Deposited from 525-Degrees-C to 725-Degrees-C. *J. Electrochem. Soc.* **1982**, *129*, 2326−2331.
(33) Kamins, T. I. *Polycrystalline Silicon for Integrated Circuit Applications*; Kluwer Academic Publishers: Boston, 1988.
(34) Hatalis, M. K.; Greve, D. W. Large Grain Polycrystalline Silicon by Low-Temperature Annealing of Low-Pressure Chemical Vapor-Deposited Amorphous-Silicon Films. *J. Appl. Phys.* **1988**, *63*, 2260−2266.
(35) Hatalis, M. K.; Greve, D. W. Thin-Film Transistors in Low-Temperature Crystallized Amorphous-Silicon Films. *J. Electrochem. Soc.* **1987**, *134*, C125−C125.
(36) Hatalis, M. K.; Greve, D. W. High-Performance Thin-Film Transistors in Low-Temperature Crystallized Lpcvd Amorphous-Silicon Films. *IEEE Electron Device Lett.* **1987**, *8*, 361−364.
(37) Spinella, C.; Lombardo, S.; Priolo, F. Crystal grain nucleation in amorphous silicon. *J. Appl. Phys.* **1998**, *84*, 5383−5414.
(38) Haji, L.; Joubert, P.; Stoemenos, J.; Economou, N. A. Mode of Growth and Microstructure of Polycrystalline Silicon Obtained by Solid-Phase Crystallization of an Amorphous-Silicon Film. *J. Appl. Phys.* **1994**, *75*, 3944−3952.
(39) Schins, W. J. H.; Bezemer, J.; Holtrop, H.; Radelaar, S. Recrystallization of Polycrystalline Cvd Grown Silicon. *J. Electrochem. Soc.* **1980**, *127*, 1193−1199.
(40) Thompson, C. V. Grain-Growth in Thin-Films. *Annu. Rev. Mater. Sci.* **1990**, *20*, 245−268.
(41) Finlayson, C. E.; Amezcua-Correa, A.; Sazio, P. J. A.; Baril, N. F.; Badding, J. V. Electrical and Raman characterization of silicon and germanium-filled microstructured optical fibers. *Appl. Phys. Lett.* **2007**, *90*, 132110.
(42) Healy, N.; Mailis, S.; Bulgakova, N. M.; Sazio, P. J. A.; Day, T. D.; Sparks, J. R.; Cheng, H. Y.; Badding, J. V.; Peacock, A. C. Extreme electronic bandgap modification in laser-crystallized silicon optical fibres. *Nat. Mater.* **2014**, *13*, 1122−1127.
(43) Richter, H.; Wang, Z. P.; Ley, L. The One Phonon Raman-Spectrum in Microcrystalline Silicon. *Solid State Commun.* **1981**, *39*, 625−629.
(44) Peacock, A. C.; Mehta, P.; Horak, P.; Healy, N. Nonlinear pulse dynamics in multimode silicon core optical fibers. *Opt. Lett.* **2012**, *37*, 3351−3353.
(45) English, T. S.; Smoyer, J. L.; Duda, J. C.; Norris, P. M.; Beecham, T. E.; Hopkins, P. E. *Modeling grain boundary scattering and thermal conductivity of polysilicon using an effective medium approach*; 8th Thermal Engineering Joint Conference, ASME/JSME, 2011.

DOI: 10.1021/acsphotonics.5b00434
ACS Photonics 2016, 3, 378−384

(46) Claps, R.; Dimitropoulos, D.; Raghunathan, V.; Han, Y.; Jalali, B. Observation of stimulated Raman amplification in silicon waveguides. *Opt. Express* **2003**, *11*, 1731−1739.
(47) Shen, L.; Healy, N.; Mehta, P.; Day, T. D.; Sparks, J. R.; Badding, J. V.; Peacock, A. C. Nonlinear transmission properties of hydrogenated amorphous silicon core fibers towards the mid-infrared regime. *Opt. Express* **2013**, *21*, 13075−13083.

DOI: 10.1021/acsphotonics.5b00434
ACS Photonics 2016, 3, 378−384